Journal of the Physical Society of Japan
Vol. 53, No. 12, December, 1984, pp. 4138–4154

Phase Transition of the Two-Dimensional Heisenberg Antiferromagnet on the Triangular Lattice

Hikaru KAWAMURA and Seiji MIYASHITA†

Department of Physics, College of General Education, Osaka University, Toyonaka 560, Osaka
†*Department of Physics, Faculty of Science, Tokyo University, Tokyo 113*

(Received July 26, 1984)

Ordering process of the antiferromagnetic Heisenberg model on the two-dimensional triangular lattice is studied both by topological analysis of defects and by Monte Carlo simulation. It is shown that the order parameter space of this model is isomorphic to the three-dimensional rotation group SO(3) due to the inherent frustration effect. Homotopy analysis shows that the system bears a topologically stable point defect characterized by a two-valued topological quantum number and exhibits a phase transition driven by the dissociation of the vortices. A Monte Carlo study on the specific heat and the behavior of vortices strongly suggests the occurence of a Kosterlitz-Thouless-type phase transition. It is, however, argued that in contrast to the two-dimensional XY model, the spin-correlation function decays exponentially even in the low-temperature phase. In order to distinguish the high- and low-temperature phases qualitatively, we introduce a "vorticity function" analogously to the Wilson loop in the quark-confinement problem in the lattice gauge theory. A discussion is made on possible interpretations of the experimental data for triangular lattice Heisenberg antiferromagnets.

§1. Introduction

It has recently been recognized that the frustration effect plays an important role in various kinds of magnetic systems. In particular, antiferromagnets on the triangular lattice (AFT model) give typical examples of such frustrated spin systems. Recent active studies have revealed that these systems show quite different behavior from that of the corresponding ferromagnetic models reflecting the fully frustrated nature of the lattice.

The phase transition of the AFT model also depends on the symmetry of the interaction. For the Ising model,[1-6] the frustration effect tends to cause a degeneracy of the ground state. Especially when the interaction is restricted to nearest neighboring spins, the ordering is seriously suppressed by the frustration effect. There exists a macroscopic ground state entropy and the system shows no phase transition at any finite temperature.[1] Inclusion of second neighbor interactions, however, turns out to enhance the sublattice ordering and the system shows successive phase transitions as the 6-state clock model or the ferromagnetic XY model with sixfold symmetry-breaking field.[7]

In the case of the AFT plane rotator (XY) model, the frustration effect causes an additional twofold degeneracy of the ground state. The ground state of this model consists of spins on three sublattices forming 120° angles, leading to a $\sqrt{3}\times\sqrt{3}$ periodicity (120° structure). Such type of ground state has a twofold discrete degeneracy as well as an XY-like continuous degeneracy. (We express the structure of such ground state by $Z_2\times S_1$ where Z_2 is a two-element group and S_1 is a one-dimensional circle.) As a consequence, this system is expected to have two different mechanisms of phase transition, i.e., the Ising-type symmetry-breaking mechanism and the Kosterlitz-Thouless mechanism with the low-temperature phase characterized by the power-law-decaying spin correlation. In fact, Monte Carlo simulations by Miyashita and Shiba[8] and by Lee, Joannopoulos, Negele and Landau[9] have shown that there actually exist the two types of mechanisms of phase transition.

In the present paper, we shall study the nature of ordering process of the isotropic *Heisenberg* AFT model.[10] Recently several interesting experiments concerning this system have been reported.[11-15] We consider the classical Heisenberg Hamiltonian given by

$$\mathcal{H}=J\sum_{\langle ij\rangle}\boldsymbol{S}_i\cdot\boldsymbol{S}_j,\quad J>0, \tag{1.1}$$

where $\boldsymbol{S}_i$ is a three-component unit vector $\boldsymbol{S}_i=(S_i^x, S_i^y, S_i^z)$ with $|\boldsymbol{S}_i|=1$, and the sum is taken over all nearest neighboring pairs. At first sight, it might seem that this model does not have any phase transition at finite temperatures, because it is widely accepted that the ferromagnetic Heisenberg model exhibits no phase transition in two dimensions[16] and the frustration effect weakens the spin ordering. In the present case, however, the situation is not necessarily so simple. In order to see this situation, let us investigate the structure of the order parameter of the present model. In the ground state of (1.1), spins are ordered in the 120° structure as illustrated in Fig. 1(a). The order parameter consists of three distinguishable arrows in a plane. Here note that in contrast to the AFT plane rotator model the plane on which 120° structure lies can take any direction in the spin space. One can see that the order parameter space V of the present model has the same structure as the orthogonal frame or the rigid body in space and is isomorphic to the three-dimensional rotation group SO(3) or the projective space P_3:[17,18]

$$V=SO(3)=P_3. \tag{1.2}$$

This space can be regarded as a three-dimensional solid sphere where diametrically opposite points on the surface are identified. This situation contrasts with the case of the ferromagnetic Heisenberg model, in which the order parameter is a single arrow (Fig. 1(b)). In the case of the antiferromagnetic Heisenberg model on the bipartite lattice, the situation is essentially the same as the ferromagnetic case (Fig. 1(c)). The order parameter space of these nonfrustrated systems is isomorphic to the two-dimensional sphere S_2,

$$V=SO(3)/SO(2)=S_2. \tag{1.3}$$

This difference originates from the structure of the order parameter which is caused by the frustration effect. Note that in both the ferromagnetic and antiferromagnetic cases each Heisenberg spin has the same degree of freedom isomorphic to S_2. In the AFT case, however, an elementary ordering unit consists of *three* spins on an elementary triangle instead of *one* spin on the lattice point. Similar situation exists also for the Ising and the plane rotator AFT models. In the Ising model with second-neighbor interactions, a twofold degeneracy of a single spin Z_2 is changed into a sixfold one Z_6, and in the plane rotator model the degree of freedom of a single spin S_1 is doubled into $Z_2\times S_1$. The order parameter spaces for various continuous spin systems on the two-dimensional triangular lattices are summarized in Table I. We note that the same order parameter as that of the present model appears in the superfluid A phase of ^{3}He[19] and in amorphous structure in glasses.[20]

Above analysis shows that the order param-

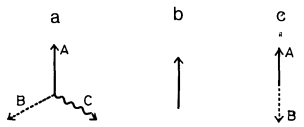

Fig. 1. Order parameter of the Heisenberg antiferromagnet on the triangular lattice (a), the Heisenberg ferromagnet (b) and the antiferromagnet on the bipartite lattice (c). Symbols A-C represent each sublattice of the original lattice.

Table I. Table of the order parameter spaces and the associated homotopy groups for various continuous spin systems on the two-dimensional triangular lattice.

	V	Π_0(V)	Π_1(V)	Π_2(V)
Model	Order parameter	Line	Point	Instanton
Ferro *XY*	$S_1=SO(2)$	0	Z	0
Ferro Heisenberg	S_2	0	0	Z
AF. *XY*	$Z_2\times S_1$	Z_2	Z	0
AF. Heisenberg	$P_3=SO(3)$	0	Z_2	0

eter of the Heisenberg AFT model is quite different from the one of the corresponding ferromagnetic model. Therefore, there exists a possibility that the present model shows a phase transition which might belong to a new universality class. In the following, we shall study the nature of ordering process of the AFT Heisenberg model making use of a topological argument for defects and also a Monte Carlo simulation.

It is found that the present model bears a topologically stable point defect—vortex. In contrast to the usual vortex which we see in the two-dimensional XY model, the present vortex is characterized by a two-valued topological quantum number (Z_2 vortex). As well as the usual vortices, the Z_2 vortices turn out to form bound pair at low temperatures and begin to dissociate at a certain critical temperature causing a Kosterlitz-Thouless-type phase transition. In contrast to the XY model, in the present model continuous deformations (spin waves) destruct the spin ordering so that the spin correlation is expected to fall off exponentially even in the low-temperature phase. Consequently, the phase transition takes place between the two phases both of which have exponentially-decaying spin correlations. We have found that an "order parameter" of the present model, which characterizes the high- and low-temperature phases qualitatively, can be introduced through a "vorticity function" which has an analogous structure to the Wilson loop which is familiar in the quark-confinement problem in the lattice gauge theory.[21] The vorticity function decays by the area law in the high-temperature phase and by the perimeter law in the low-temperature phase, thus showing the existence of distinct high- and low-temperature phases.

This paper is organized as follows: In §2, we investigate topologically stable defects of the present model by means of homotopy analysis. In §3, the nature of phase transition is discussed on the basis of the vortex bound-unbound picture. In §4, we present results of Monte Carlo simulation to confirm our scenario for the nature of phase transition and the low-temperature phase. Section 5 is devoted to summary and discussion.

§2. Topological Analysis of Defects

Assuming the 120° structure, we have shown that the order parameter space of the AFT Heisenberg model is isomorphic to $V=SO(3)=P_3$. To proceed further, let us investigate the topologically stable defect of the present model, that is the defect which cannot be eliminated by operating the continuous transformation corresponding to the spin wave. Mathematically this can be done by studying the r-th homotopy group of the order parameter space $\Pi_r(V)$.[17,18] In the present case, they are given by

$$\Pi_0(P_3)=0, \quad \Pi_1(P_3)=Z_2, \quad \text{and} \quad \Pi_2(P_3)=0. \tag{2.1}$$

When the spatial dimension is equal to two, the relations (2.1) mean that the system has no topologically stable line defect ($\Pi_0=0$) nor instanton ($\Pi_2=0$), but has stable point defect ($\Pi_1=Z_2$). For details of the homotopy analysis of defects, we refer the reader to ref. 19. In the real space, this point defect has a vortex-like configuration as is illustrated in Fig. 2(a) or (b). In this example, all spins lie on a common plane and each 120° structure rotates clockwise (Fig. 2(a)) or counterclockwise (Fig. 2(b)) when one makes a clockwise turn around the vortex core. However, the apparent distinction between Figs. 2(a) and 2(b) is a spurious one as is shown below. The usual vortex which we see in the two-dimensional XY model can be labeled by integers, 0, ±1, $\pm2,\cdots$(vortex number) corresponding to the nature of the point defect $\Pi_1(S_1)=Z$, (S_1; the order parameter space of the XY model). On the other

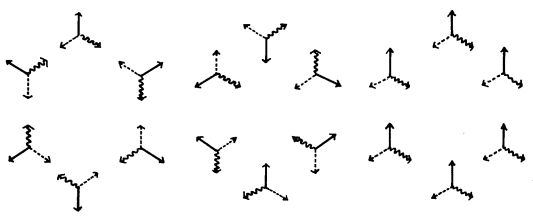

Fig. 2. An example of vortex configuration. Configuration (a) can be continuously transformed into (b) and vice versa, but neither (a) nor (b) can be continuously transformed into (c). The chirality vector defined by (2.2) is perpendicular to the plane of the page for all configurations.

hand, the present vortex is labeled only by ± 1 due to the Z_2 structure, which we call "oddness" or "parity". In Figs. 2, "vortex" (Fig. 2(a)) can be continuously transformed into "antivortex" (Fig. 2(b)) by 180° rotation of each spin plane on which the 120° structure lies. Here we should note that it is impossible to change the single vortex (Fig. 2(a) or 2(b)) into the vortex free configuration (Fig. 2(c)), which indicates that the Z_2 vortex is a topologically stable defect. In Table I, we summarize topologically stable defects of various continuous spin systems on the triangular lattice. We note that in contrast to the AFT Heisenberg model the *ferromagnetic* Heisenberg model cannot bear a vortex while it has an instanton which is a topological excitation without singularity in two dimensions.

In the above example (Figs. 2), we take a vortex structure for which all spins are on a plane for an example, but of course there are various realizations of the Z_2 vortex in the Heisenberg model where spins are not restricted on a plane. We introduce another typical example which is illustrated in Fig. 3, where the spins on one sublattice are fixed to be vertical to the plane of the page and spins on the other two sublattices rotate making a vortex. Hereafter, we shall refer the two types of vortices shown in Figs. 2 and 3 as type I and type II vortices, respectively. Now let us introduce a vector "chirality" which is defined on each upward elementary triangle by

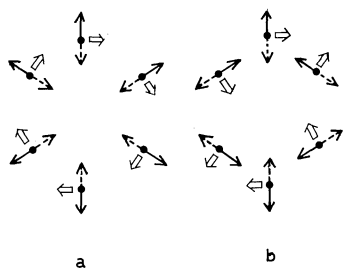

Fig. 3. Another example of vortex configuration, where spins on one sublattice are perpendicular to the plane of the page while spins on other two sublattices rotate around this axis. The chirality vectors defined by (2.2) lie on the plane of the page and rotate clockwise (a) or counterclockwise (b) when one makes a clockwise turn around the vortex core. Configuration (a) can be continuously transformed into configuration (b) and vice versa.

$$\boldsymbol{\kappa}=\frac{2}{3\sqrt{3}}(\boldsymbol{S}_1\times\boldsymbol{S}_2+\boldsymbol{S}_2\times\boldsymbol{S}_3+\boldsymbol{S}_3\times\boldsymbol{S}_1), \tag{2.2}$$

where the corner sites 1, 2 and 3 are numbered counterclockwise for an upward elementary triangle. This vector is vertical to the plane on which the 120° structure lies, and its length gives a measure of the rigidity of the 120° structure. It is normalized to give unity for a complete 120° structure and vanishes when any two spins on an elementary triangle is parallel. The above definition of the chirality is formally identical with the one introduced for the AFT plane rotator model,[8] but $\boldsymbol{\kappa}$ is a three-dimensional vector in contrast to the case of the plane rotator model where it is an axial scalar. In the type I vortex the chirality vectors are fixed to be perpendicular to the plane of the page, whereas in the type II vortex the chirality vectors rotate around the vortex core. In order to determine which type of vortices are dominant in thermal equilibrium, it is necessary to estimate the energy of each vortex. We have evaluated the energy of a single vortex both for the type I and II vortices within the continuum approximation. The results are given by

$$E_{\mathrm{I}}/J\simeq 2\sqrt{3}\pi\ln\frac{L}{d}, \tag{2.3}$$

$$E_{\mathrm{II}}/J\simeq\sqrt{3}\pi\ln\frac{L}{d}, \tag{2.4}$$

where L is a linear dimension of the system and d is a lattice cutoff. The logarithmic dependence on the system size is found in common with the usual vortex in the two-dimensional XY model. This size dependence should be contrasted to the case of instantons in the ferromagnetic Heisenberg model which has a finite excitation energy independent of the system size. Because the type II vortex has a lower energy than the type I vortex, it is expected that the type II vortex is dominant in thermal equilibrium and the Z_2 vortex can be regarded as a vortex formed by chirality vectors. An example of the Z_2 vortex observed in a Monte Carlo simulation is shown in Fig. 4, where a snapshot of an equilibrium spin configuration (Fig. 4b) and the corresponding snapshot of chirality configuration (Fig. 4(a)) are shown. The Z_2 vortex in the present model can actually be regarded as a vortex formed by chirality

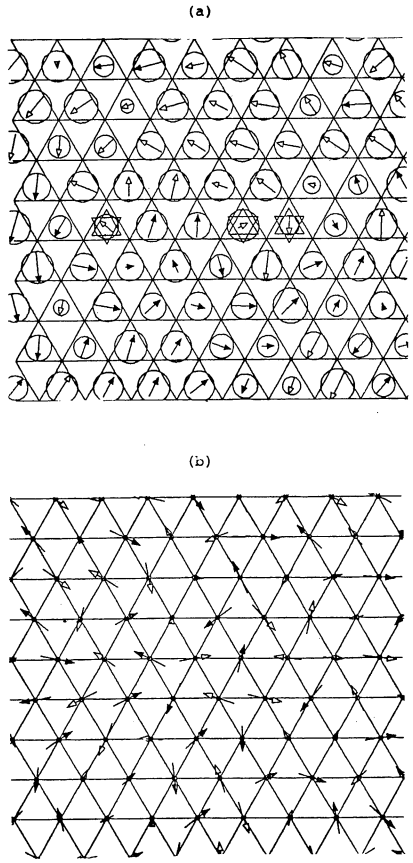

Fig. 4. A typical snapshot of vortex configuration observed in a Monte Carlo simulation. Chirality vectors and vortex positions are given in Fig. (a) and the corresponding spin configurations are given in Fig. (b). Arrows with open triangles denote vectors in upward directions whereas arrows with solid triangles denote vectors in downward directions. In Fig. (a), the radius of a circle represents the length of each chirality vector and the symbol ✡ denotes the vortex position. This shot is taken after waiting for 5000 MCS starting from a complete random spin configuration, and the system is supposed to be in thermal equilibrium. The temperature is $T/J=0.33$.

vectors.

At this point, we give a definition of the "vorticity". First assume that ideal 120° structure is assigned on every elementary triangle. Though the 120° structure is not rigid at any finite temperature due to the thermal disturbance, it is not so unreasonable to expect that the system has an enough degree of short-range order so that one can reasonably assign the 120° structure via an averaging procedure. (We shall check the validity of this assumption in §4 by means of Monte Carlo simulation.) Let us consider the dual lattice of upward elementary triangles which makes $\sqrt{3}\times\sqrt{3}$ structure on the original triangular lattice (see Fig. 5). We consider the 120° structures on the dual lattice points and define "rotation" between the 120° structures at each directed link on the dual lattice. One can specify each rotation by the rotation angle ω and the rotation axis $\hat{\boldsymbol{n}}$ ($|\hat{\boldsymbol{n}}|=1$). In order to detect the vortex structure, we represent a rotation with use of the SU(2) matrix. As is known SU(2) is a two-valued representation of SO(3) so that a rotation by 2π can be distinguished from a rotation by 0 (no rotation). Generally a rotation by $(\omega, \hat{\boldsymbol{n}})$ can be represented by the following two SU(2) matrices of mutually opposite sign:

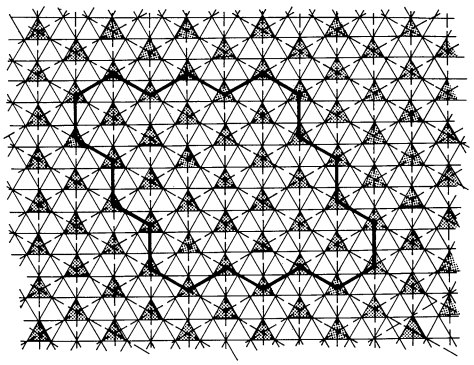

Fig. 5. Triangular lattice and its dual lattice. Thin line represents the original triangular lattice on which Heisenberg spins are put. Shaded triangles represent upward elementary triangles on which the 120° structures are assigned. Broken line represents the dual triangular lattice which makes $\sqrt{3}\times\sqrt{3}$ structure on the original triangular lattice. An example of a closed contour on the dual lattice is also shown with the bold line.

$$U=\pm\exp\left(\frac{\omega}{2i}\hat{\boldsymbol{n}}\cdot\boldsymbol{\sigma}\right), \tag{2.5}$$

where $\boldsymbol{\sigma}=(\sigma_x, \sigma_y, \sigma_z)$ are Pauli matrices. These two SU(2) matrices can be interchanged each other by the replacement $\omega\rightleftarrows 2\pi-\omega$ and $\hat{\boldsymbol{n}}\rightleftarrows -\hat{\boldsymbol{n}}$. It is therefore possible to choose a SU(2) matrix with the condition $-\pi<\omega\leq\pi$. Thus one can uniquely assign a SU(2) matrix U_i on every directed link on the dual lattice, which can be regarded as a link variable. Let us consider a closed contour C on the dual lattice and construct a product of all SU(2) matrices

around closed path of links:

$$\prod_{i\in C} U_i = U_N U_{N-1} \cdots U_2 U_1. \tag{2.6}$$

Note that the order of U_i's is important because SU(2) is a non-abelian group. From the definition (2.6), it is apparent that this quantity is equal to either I or $-$I where I is a 2×2 unit matrix. Then we can define the vorticity associated with a closed contour C by

$$V[C] = \frac{1}{2} T_r \left(\prod_{i\in C} U_i\right). \tag{2.7}$$

The voriticity $V[C]$ takes only two values, unity or minus unity. When $V[C]$ is equal to unity, the contour C involves no net vorticity, whereas when it is equal to minus unity it bears a net vorticity. This two-valuedness of the vorticity corresponds to the aforementioned Z_2 nature of the vortex. From the definition (2.7), we have the conservation law of the vorticity. If a closed contour C consists of two parts C_1 and C_2 each of which has a vorticity $V[C_1]$ and $V[C_2]$, the total vorticity is given by $V[C]=V[C_1]V[C_2]$, while the conservation law for the usual vortex (Z vortex) holds via the addition of vortex number. Therefore, once the vorticity is known for every plaquette, the vorticity of any closed contour can be calculated by simple multiplication of vorticities for all plaquettes in the region surrounded by the contour.

§3. Phase Transition

The excitation energy of an isolated vortex is proportional to ln L as is shown in (2.4) and becomes infinite in the thermodynamic limit. Therefore, the probability of finding the free vortex is vanishingly small at low temperatures and vortices exist only as a tightly bound vortex pair. At higher temperatures, a contribution of the entropy is also relevant which is estimated as

$$S \simeq k_B \ln \left(\frac{L}{d}\right)^2. \tag{3.1}$$

Combining (2.4) with (3.1), one can expect a critical temperature $k_B T_c \simeq \sqrt{3}\pi/2$ above which spontaneous generation of free vortices takes place. This is just the scenario originally proposed by Kosterlitz and Thouless[22] for the phase transition of the two-dimensional XY model. The only difference is that the present vortex is characterized by its "parity" (Z_2) not by "charge" (Z). However, as the energetical situation is the same for the both models, one can expect the Kosterlitz-Thouless transition[22] associated with the Z_2 vortices in the present model, i.e., at the critical temperature Z_2-vortex pairs begin to dissociate and the free vortices appear at higher temperatures. One important difference is expected in the behavior of the spin-correlation function in the low-temperature phase. In the low-temperature phase of the XY model, the spin-correlation function decays algebraically accompanied with the divergent susceptibility.[22] In the present case, on the other hand, the remaining spin wave freedom associated with Heisenberg spin is sufficient to destroy the spin ordering and the spin-correlation function decays exponentially even in the low-temperature phase. Intuitively, the degree of freedom S_2 of the chirality which survives below T_c, is enough to destroy the spin ordering. In the case of the *ferromagnetic* Heisenberg model whose order parameter space is S_2, it has also been shown that the spin-correlation function decays exponentially at any finite temperature.[16] In this system, however, the Kosterlitz-Thouless mechanism of phase transition does not work beeause the topological excitation, instanton, has only *finite* energy.

In order to investigate the nature of the low-temperature phase and the phase transition from the symmetry viewpoint, we further go on our topological argument. First, let us consider an example of the ferromagnetic XY model which exhibits the Kosterlitz-Thouless transition and whose low-temperature phase can be characterized by the disappearance of free vortices. The effective symmetry of this low-temperature state can be represented by the space constructed from the original order parameter space by eliminating the vortex freedom without changing the other degrees of freedom. Mathematically this procedure corresponds to making the order parameter space to be *simply connected*, preserving the local properties of the space. In the topological language, this corresponds to taking the *universal covering* of the original space. In the case of the XY model, the universal covering of the original order parameter space is $\bar{S}_1 = R_1 = T(1)$, i.e.,

the straight line or the one-dimensional translational group. The low-temperature phase of the XY model can be actually well approximated by the harmonic Hamiltonian in which variables are permitted to take any real value corresponding to R_1, where the spin-correlation function decays algebraically $\langle\cos(\phi_i-\phi_j)\rangle\propto r_{ij}^{-\eta}$, that is the angle deviation diverges logarithmically to the distance, $\langle(\phi_i-\phi_j)^2\rangle\propto\eta\log r_{ij}$, irrespectively of the original 2π modulus of the angle. We may say that the phase transition of the XY model can be characterized by the symmetry change: $S_1\rightleftarrows T_1$.

In the case of the present model, the low-temperature phase can be characterized by the disappearance of the free Z_2 vortices. The universal covering of the order parameter space is $\bar{P}_3=S_3$, i.e., the three-dimensional sphere which is also the order-parameter space of the 4-component ferromagnetic Heisenberg model. Consequently, we may say that the phase transition of the present model is characterized by the symmetry change: $P_3\rightleftarrows S_3$. Noting the fact that the spin-correlation function decays exponentially at any finite temperature in the O(4) Heisenberg model in two dimensions, we expect that the spin-correlation function of the present model decays exponentially even in the low-temperature phase, which is consistent with our previous intuitive discussion. Then the correlation length of the spin correlation of the present model does not diverge at T_c, though it will grow rapidly around T_c reflecting the disappearance of the free vortices.

For two-dimensional spin systems with continuous symmetry, the absence of long-range order is rigorously proved.[23] Moreover, we have argued that the spin-correlation function of the present model decays exponentially at any finite temperature in contrast to the two-dimensional XY model. Then a question naturally arises what is the physical quantity which can qualitatively distinguish the high- and low-temperature phases of the present model. In other words, what is an "order parameter" which is directly relevant to the present phase transition? We shall show that the order parameter of the present model can be defined via the asymptotic behavior of the thermal average of the vorticity (2.7).

Consider a closed contour C which is much larger than a lattice spacing but much smaller than the system size. Let the perimeter of this contour be R ($d\ll R\ll L$). In the limit $R\to\infty$, the thermal average of the vorticity goes to zero at any non-zero temperature. It is, however, expected that its asymptotic behavior for $R\to\infty$ characterizes the high- and low-temperature phases. In fact, we have found

$$V_R=\langle V_R[C]\rangle\underset{R\to\infty}{\to}\begin{cases}\exp(-\alpha A) & (T>T_c)\\ \exp(-\beta R), & (T<T_c)\end{cases} \tag{3.2}$$

where A is the area of the region surrounded by the contour C. The derivation of (3.2) is given in Appendix. Hereafter we shall call V_R "vorticity function". Above T_c, the vorticity function falls off rapidly by the *area law*, whereas below T_c it falls off rather slowly by the *perimeter law*. We note that this criterion of phase transition is quite analogous to the one familiar in the quark-confinement problem in the lattice Gauge theory.[21] The vorticity function corresponds to the Wilson loop, and the high- and low-temperature phases in the present model correspond to the confined and deconfined phases in the lattice Gauge theory, respectively. The asymptotic behavior of the vorticity function can also be summarized in the form:

$$V_R\sim\exp(-\alpha R-\beta A). \tag{3.3}$$

Below T_c, β is equal to zero leading to the perimeter law, and above T_c, β becomes finite leading to the area law. Thus, we may call β a disorder parameter of the present model, i.e., it is zero or nonzero depending on whether the temperature is below or above T_c. In contrast to β, α is expected not to show a remarkable temperature dependence around T_c.

§4. Monte Carlo Simulation

In order to see whether the above argument of the phase transition for the present model actually holds or not, we have carried out a Monte Carlo study for the model Hamiltonian (1.1). The size of the system is $L\times L$ with $L=18$, 24, 30, 36, 45 with periodic boundary condition. The procedure of our simulation is as follows.[24] First a site is chosen at random, and a new direction of the spin on this site is

chosen at random. We determine whether this new direction of the spin is accepted or not according to the standard Metropolis rule. If it is not accepted, the spin is rotated at random around a local molecular-field axis, that is a precessional motion is made. After discarding initial 5000 Monte Carlo steps per spin (MCS) for equilibration, subsequent 40000–60000 MCS are used to calculate the average.

In Fig. 6, we show the temperature dependence of the internal energy together with the result of the harmonic approximation $E=-(3/2)J+k_BT$. (This result is obtained by applying the equi-partition law to the independent degrees of freedom associated with Heisenberg spins, that is two modes per spin.) The temperature dependence of the specific heat calculated from the energy fluctuation is shown in Fig. 7 and in Table II. It shows a sharp peak at $k_BT/J\simeq 0.33$. Though a weak size dependence is found in the range $12\leq L\leq 36$, the peak height seems to saturate at the largest sample $L=45$, and is certainly non-divergent. This fact suggests that the apparent size dependence observed in smaller samples is due to the onset of short-range order. This interpretation is consistent with the data for the sublattice magnetization which will be shown below. We note that the temperature dependence of the specific heat is quite similar to the one found in the ferromagnetic plane

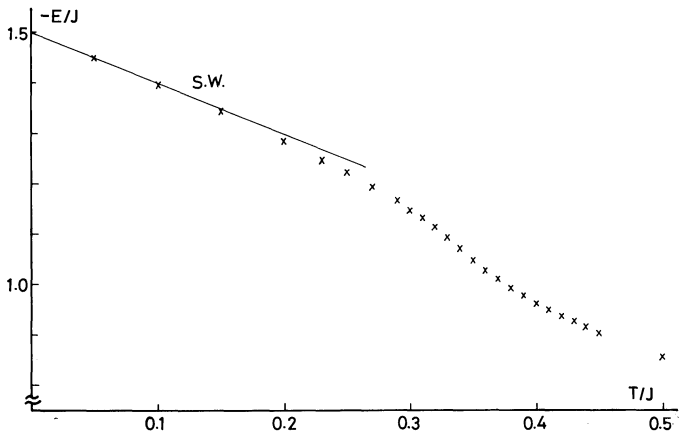

Fig. 6. Temperature dependence of the internal energy. The solid line denotes the low-temperature behavior expected from the harmonic approximation. The lattice size is $L=24$.

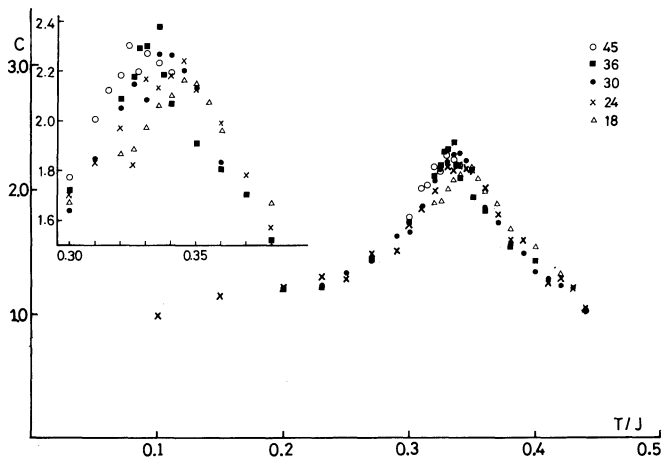

Fig. 7. Temperature dependence of the specific heat evaluated from the energy fluctuation. The inset shows the same result in a magnified scale to emphasize the size dependence.

Table II. The temperature and size dependence of the specific heat. The statistical error represents the first standard deviation over 2–4 independent runs. The data shown without statistical error is taken from a single run. The average values are plotted in Fig. 7.

T/J	L				
	18	24	30	36	45
0.5		0.9087	0.8782	0.8528	
0.45		1.0536	1.0474		
0.44		1.0221	1.1082		
0.43		1.1814	1.1876		
0.42	1.3110	1.2720	1.2108		
0.41	1.6563	1.2262	1.2722		
0.40	1.5188	1.3201	1.3178	1.3954	
0.39		1.5724	1.4676		
0.38	1.6724	1.5703±0.0465	1.5480	1.5177	
0.37	1.8701±0.0323	1.7786±0.0290	1.7073		
0.36	1.9605±0.0494	1.9888±0.0669	1.8325±0.0295	1.8084	
0.355	2.0737				
0.35	2.1540±0.0880	2.1233±0.0683	2.1329±0.0871	1.9131	
0.345	2.1652	2.2414	2.2005±0.0276		
0.34	2.1027±0.0869	2.1785±0.1209	2.2656±0.0048	2.0686	2.1926
0.337				2.1837	
0.335	2.0584	2.1310±0.0439	2.2670±0.0074	2.3767±0.0385	2.2325
0.33	1.9756±0.0574	2.1662±0.1572	2.2084±0.0552	2.2980±0.0553	2.2725
0.327				2.2949	2.1993
0.325	1.8755	1.8200±0.1096	2.1458	2.1751	2.1430
0.323					2.3022
0.32	1.8706±0.0552	1.9711±0.1095	2.0544	2.0870	2.1834
0.315					2.1226
0.31		1.8313	1.8494		2.0072
0.30	1.6760	1.7015	1.6394±0.0211	1.7222	1.7726
0.29		1.4922	1.6073		
0.27		1.4696	1.4093	1.4115	
0.25		1.2705	1.3216		
0.23		1.2852	1.2168	1.2974	
0.20		1.2020	1.1977	1.1978	
0.15		1.1309			
0.10		0.9789			

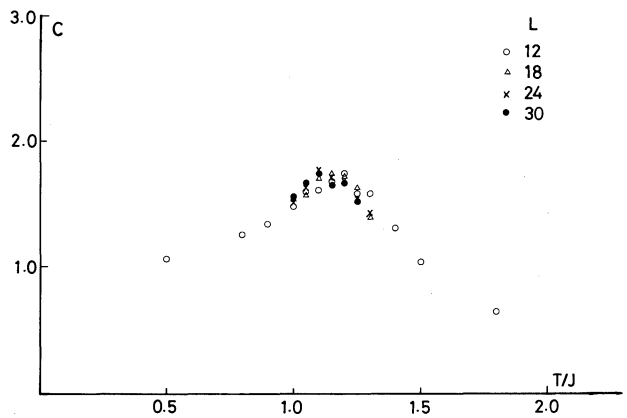

Fig. 8. Temperature dependence of the specific heat of the ferromagnetic Heisenberg model on the triangular lattice evaluated from the energy fluctuation.

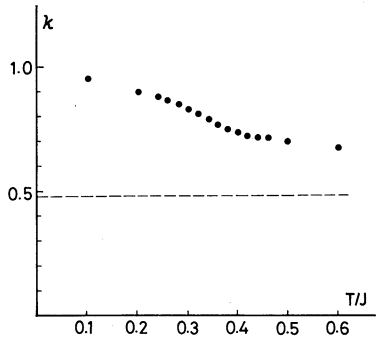

Fig. 9. Temperature dependence of the average length of the local chirality vector $\kappa=\langle|\boldsymbol{\kappa}_i|\rangle$. Dashed line represents the value in the high temperature limit. The lattice size is $L=30$.

rotator model,[25,26] which suggests the occurrence of the Kosterlitz-Thouless transition of the Z_2 vortices for the present model. For comparison, we also show in Fig. 8 the temperature dependence of the specific heat of the *ferromagnetic* Heisenberg model on the triangular lattice. It shows a maximum at $k_BT/J\simeq 1.1$, but the peak seems much broader as compared with the antiferromagnetic case.

In Fig. 9, we show the temperature dependence of the average length of the local chirality vector $\kappa=\langle|\boldsymbol{\kappa}_i|\rangle$. This quantity is about equal to 0.48 in the high-temperature limit, but it takes a value 0.7–0.8 near the temperature where the specific heat is maximum, indicating that the approximate 120° structure still exists around the temperature range of interest. Making use of the short-range order, we have assigned the rigid 120° structure, or equivalently the orthogonal frame, to each elementary triangle discarding the thermal disturbances. In practice, we have extracted two orthogonal unit vectors from a given configuration of three spin vectors on each elementary triangle according to the following procedure: One unit vector $\boldsymbol{n}_1$ is chosen as parallel with the chirality vector (2.2) on the elementary triangle. The second unit vector $\boldsymbol{n}_2$ is chosen to satisfy the relations $\boldsymbol{n}_1\cdot\boldsymbol{n}_2=0$ and $(\boldsymbol{n}_1\times\boldsymbol{n}_2)\cdot\boldsymbol{S}_i=0$ where $\boldsymbol{S}_i$ is the spin vector on one specified sublattice A, $i\in A$. Thus determined two unit vectors can uniquely designate the 120° structure at each elementary triangle. Once the rigid 120° structures are assigned, the total number of elementary vortices can be calculated by counting the vorticity at each unit plaquette on the lattice. The total number of Z_2 vortices is always even which is required from the periodic boundary condition. In our simulation, the number density of elementary Z_2 vortices n_v is calculated on a 30×30 lattice by averaging 200 samples which are taken every 10 MCS after discarding initial 5000 MCS. The temperature dependence of n_v is shown in Fig. 10(a), where a sharp drop-off of the density is observed near the specific heat maximum. In Fig. 10(b), we plot $\ln n_v$ versus J/T. At low temperatures, $\ln n_v$ is proportional to J/T with a slope being -3.3, and the chemical potential of a vortex pair is estimated as $2\mu\sim 3.3\,J$ which is smaller than the corresponding value in the ferromagnetic plane rotator model on the square lattice $2\mu\sim 10.2\,J$.[26] Near the specific

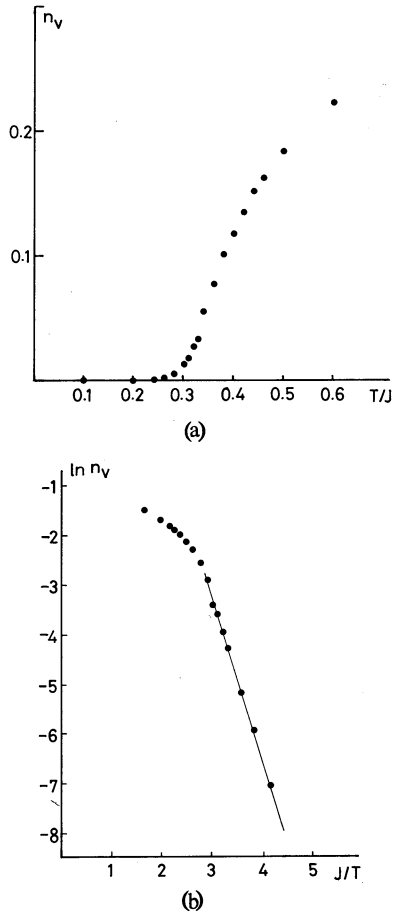

Fig. 10. Temperature dependence of the number density of the Z_2 vortices: (a) n_v vs. J/T and (b) $\ln n_v$ vs. J/T. The lattice size is $L=30$.

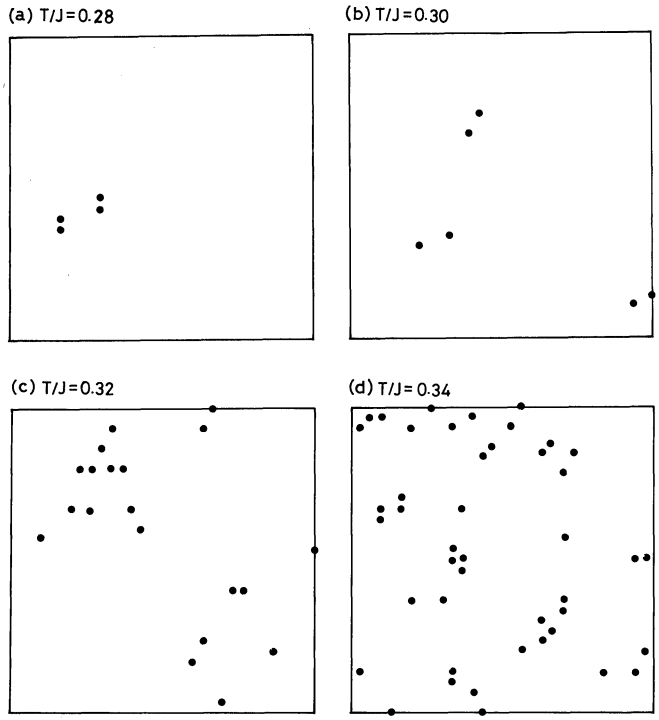

Fig. 11. Typical snapshots of the Z_2 vortex configuration both below and above T_c: (a) $T/J=0.28$, (b) $T/J=0.30$, (c) $T/J=0.32$ and (d) $T/J=0.34$. The lattice size is $L=30$.

heat maximum the curve levels off indicating that the effective excitation energy of the vortex becomes smaller due to the screening effect by other vortices. In Fig. 11, we display typical snapshots of vortex configurations for several temperatures between $T/J=0.28$ and 0.34. As expected, Z_2 vortices form tightly bound vortex pairs at low temperatures. As the temperature increases, both the number of pairs and the separation between the members of a pair increases. At $T/J=0.32$, a pair with its separation considerably larger than a lattice spacing appears confirming the vortex bound-unbound mechanism of the phase transition. Note that there is a tendency that the vortices form clusters consisting of more than two vortices. At $T/J\geq 0.34$, more vortices appear and the identification of distinct pairs or clusters becomes difficult. From Figs. 10–11, one can see that the vortices in the present model behave in quite an analogous manner to the vortices in the ferromagnetic XY model,[25,26] aside from the fact that in the present case the distinction between the vortex and the antivortex is absent. This observation strongly suggests the occurrence of a Kosterlitz-Thouless-type phase transition which is driven by the dissociation of Z_2-vortex pairs.

As has been discussed in §3, the quantity which is directly relevant to the phase transition is the asymptotic behavior of the vorticity function V_R. In order to investigate this quantity, we consider a closed contour of a square form which has in total $4R$-2 edges and $3R^2/2$ plaquettes with the geometry shown in Fig. 5 with the bold line. The size dependence of V_R is examined by changing R from 2 to 30 in a 60×60 lattice. After discarding initial 5000 MCS, subsequent 100–200 samples taken every 10 MCS are averaged. The spatial average is performed at each step over all possible contours of size R in the lattice. The size dependence of V_R is shown in Fig. 12(a) at several temperatures. In Fig. 12(b), $\ln V_R/R$ is plotted versus R, which should give a horizontal line if V_R decays by the perimeter law and give a straight line with a finite tangent if V_R decays by the area law. In other words, the tangent of the asymptotic straight line gives the disorder parameter β in (3.2). Clearly, the data for

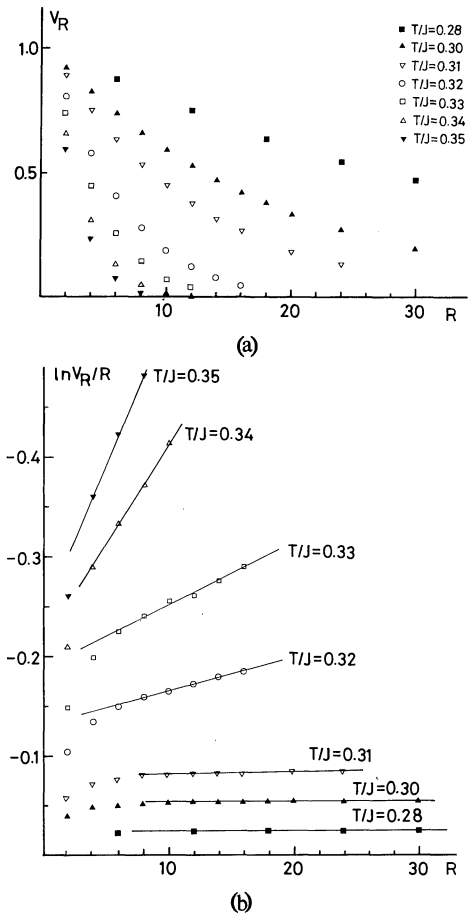

Fig. 12. Size dependence of the vorticity function: (a) V_R vs. R and (b) $-\ln V_R/R$ vs. R, where R is the perimeter of the contour. The lattice size is $L=60$. The contour has a square form which has in total $4R$-2 edges with its geometry shown in Fig. 5 with the bold line.

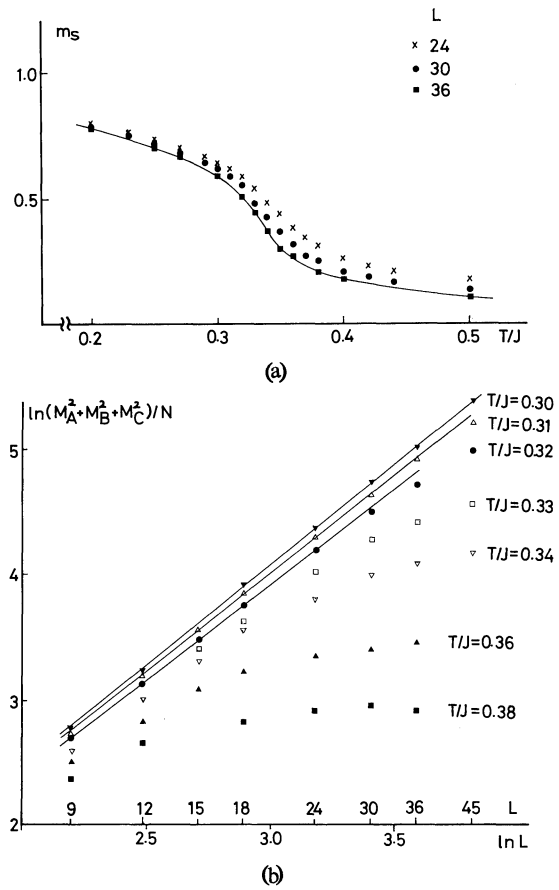

Fig. 13. Temperature dependence of the mean-square root of the sublattice magnetization (4.1) (a), and the size dependence of the squared-sublattice magnetization (b).

$T/J \leq 0.30$ become R independent for larger R indicating the perimeter law, whereas the data for $T/J \geq 0.34$ lie on straight lines with finite tangents indicating the area law. In the transition region, the data show a rather large fluctuation and a larger sample and a longer Monte Carlo run are desirable to obtain better precision. We tentatively locate the transition temperature from Fig. 12 and also from the behavior of vortices (Figs. 10 and 11) at $T_c/J \simeq 0.31 \pm 0.01$. Note that this value of T_c is considerably smaller than our previous estimation in §3 on the basis of a simple stability argument.

We show in Fig. 13(a) the temperature dependence of the mean-square root of the sublattice magnetization:

$$m_s = \frac{3}{N}\sqrt{\langle M_A^2 + M_B^2 + M_C^2 \rangle / 3}, \qquad (4.1)$$

where M_A, M_B and M_C are total sublattice magnetization of the three sublattices, respectively. In the thermodynamic limit, this quantity should identically vanish due to the theorem by Mermin and Wagner.[23] In fact, as can be seen from the figure, m_s tends to decrease as L increases. For finite systems, however, a rather rapid increase of m_s is observed when the temperature decreases across T_c indicating that the spins order in a relatively wide region. In order to see the size dependence of the squared-sublattice magnetization, $\log[\langle M_A^2 + M_B^2 + M_C^2 \rangle / N]$ is plotted versus $\ln L$ in Fig. 13(b). Note that for an exponentially-decaying spin correlation this quantity saturates for large

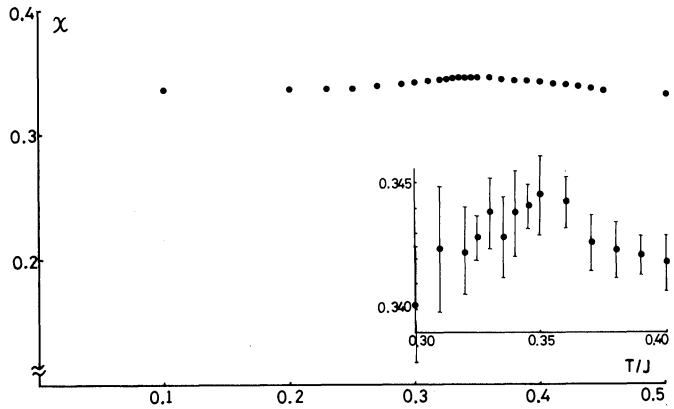

Fig. 14. Temperature dependence of the uniform susceptibility. The inset shows the same results in a magnified scale together with the scattering of the data.

enough L, whereas for a power-law-decaying spin correlation it lies on a straight line with a finite tangent. The figure shows that the data at temperatures $T/J \geq 0.31$ deviate from straight lines for larger L, whereas the data at $T/J=0.30$ lie on a straight line and cannot be distinguished from the power-law decay at least in the range $L \leq 45$. In fact, however, the spin-correlation function is expected to decay exponentially even below T_c from our argument in §3. The obtained data therefore should be interpreted as an indication of the fact that the correlation length becomes comparable with or larger than the system size around this temperature. From the data at $T/J=0.33$, the temperature at the specific heat maximum, one can see that the correlation length is roughly equal to $\xi \simeq 20$–30. This observation is consistent with the fact that the weak size dependence has been observed in the specific heat data in the range $L \leq 36$.

In Fig. 14, we show the temperature dependence of the uniform susceptibility. This quantity is almost flat in the temperature range of interest and is quite similar to the one observed in the AFT plane rotator model. We have also found that the susceptibility is almost completely isotropic even in the low-temperature phase, i.e., $\chi_{xx} \simeq \chi_{yy} \simeq \chi_{zz}$ at any temperature we studied. The observed isotropy of the susceptibility is consistent with the available experimental result.[12)]

§5. Summary and Discussion

We have investigated the triangular Heisenberg antiferromagnet and have shown that this system contains a different physics from the ferromagnetic Heisenberg model due to the inherent frustration effect. Among other things, the present model exhibits a phase transition which is driven by the dissociation of topological point defects $-Z_2$ vortices. In fact, we have found in our simulation a striking similarity in the temperature dependence of the specific heat in the behavior of vortices to the corresponding quantities of the ferromagnetic XY model, which strongly suggests the occurrence of a Kosterlitz-Thouless-type phase transition. We have argued, however, that the spin correlation function decays exponentially both below and above T_c, and the "order parameter" relevant to the phase transition is given via the asymptotic behavior of the vorticity function. This quantity obeys to the area-law above T_c and to the perimeter-law below T_c. In our simulation we have actually found a qualitative change in the asymptotic behavior of the vorticity function, and tentatively estimated the transition temperature $k_B T_c \simeq 0.31 \pm 0.01$.

Though our simulation data for the specific heat and the vorticity are strikingly similar to the ones observed in the ferromagnetic XY model, the problem still remains whether the present model belongs to the same universality class as the XY model. As the vortex in the present model possesses a different topological character from the vortex in the XY model, it might give rise to a different critical behavior. The analysis in §2 shows that the Z_2 vortex in the present model can be regarded as a vortex

formed by chirality vectors. If we neglect thermal fluctuations of long wavelength, such vortex can be specified by a rotation vector of the chirality vectors. Even when there exists a thermal disturbance due to spin waves of long wavelength, this picture of chirality vortex has a meaning inside the region of radius ξ around the vortex core, where ξ is the spin correlation length. When two Z_2 vortices come nearby with its separation much smaller than ξ, the two rotation vectors will direct in mutually opposite directions in order to lower the energy, and such Z_2 vortex pair might seem like the vortex-antivortex pair with opposite 'charge' analogous to the one found in the XY model. One can therefore expect that for a vortex pair with its separation smaller than ξ, the situation is similar to that of the XY model when the chirality vector is replaced by the spin vector. Once the separation becomes larger than ξ, however, such analogous picture does not necessarily hold because spin waves wash out all non-topological characteristics of vortices. As the phase transition is driven by the pair with *infinite* separation, the breakdown of 'charged-vortex' picture might actually affect the critical behavior of the present model. In a finite system, we must take account of the finite size effect on the critical behavior. Our simulation data show that around T_c the spin correlation length is larger than or comparable with the size of the largest system which we studied ($L=45$). If we observe a system with its size smaller than the spin correlation length at T_c, the apparent critical behavior should be similar to that of the XY model, which is consistent with the results of our Monte Carlo simulation. Thus, a possibility cannot be completely ruled out that some different aspects might appear in larger or infinite systems. Unfortunately we cannot tell at present whether the AFT Heisenberg model belongs to exactly same universality class as the XY model. This problem needs further clarification and is now under investigation.

One may note that large but finite correlation length observed in the low-temperature phase of the present model can also be seen in certain random spin systems such as spin glasses.[27] From this correspondence, it may be interesting to study the dynamical properties of the present model. As an example we show in Fig. 15 the time (Monte Carlo time) dependence of the freezing parameter (square root of the Edwards-Anderson order parameter) q for several temperatures:

$$q(t_n)=\sqrt{\frac{1}{N}\sum_i\left(\frac{1}{n}\sum_{m=1}^{n}S_i(t_m)\right)^2}. \qquad (5.1)$$

Following a rather rapid initial decay, very slow relaxation is observed in the low-temperature phase which is similar to the corresponding phenomena found in the spin glass models.[28] This fact means that the value of q depends on the time scale of observation. Experimentally informations for a single spin can be obtained by several kinds of measurements including NMR, ESR and Mösbauer spectroscopy. The typical time scale of each measurement may be estimated as $t(\mathrm{NMR})\sim 10^{-6}$ sec, $t(\mathrm{ESR})\sim 10^{-9}$ sec and $t(\mathrm{Mösbauer})\sim 10^{-7}$ sec, respectively. It means that, if the spin length can be

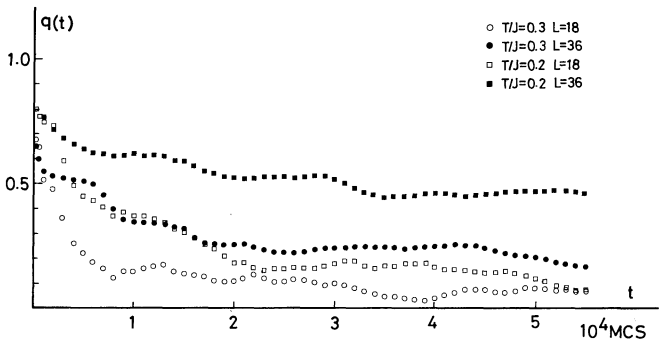

Fig. 15. Time (Monte Carlo time) dependence of the freezing parameter (square root of the Edwards-Anderson order parameter) q defined by (5.1) for $L=18$ and 36 and at temperatures $T/J=0.20$ and 0.30, respectively.

observed by each measurement, they will satisfy the following inequality:

$$q(\mathrm{ESR}) > q(\mathrm{Mösbauer, NMR}). \quad (5.2)$$

Similar situation is also expected in the spin glasses. Of course, the present model is fundamentally different from the spin glass models in some important respects. First, there exists a sharp phase transition in the present model whereas the spin glass transition is probably a dynamical one driven by the non-equilibrium effect.[27] Second, the present system is a regular system with the translational symmetry whereas the spin glass model is a random system without the translational symmetry. In this respect, the present model may be more similar to the usual glasses which is described by the translationally-invariant Hamiltonian but show very slow relaxation phenomena at low temperatures. Here it may be interesting to note that River presented a SO(3) model of glasses.[20]

It is also interesting in the present model to compare the spin length associated with a single spin, q, with the one associated with the sublattice magnetization, m_s. Experimentally the latter quantity can be measured by the neutron scattering experiment. Of course, both spin lengths should vanish in the limit of infinite observation time and infinite system size. In practice, however, both quantities give finite values because experiments measure the spin length averaged over finite time and/or over finite size. (Neutron scattering gives a sharp signal when spins are ordered over some hundreds of lattice spacing and the associated time scale is quite small $t \sim 10^{-10}$ sec.) In our simulation, the sublattice magnetization m_s is almost time independent. If we see the data for $L=36$, they are equal to $m_s \simeq 0.60$ and 0.78 at $T/J=0.30$ and 0.20, respectively. On the other hand, the freezing parameter q shows a very sluggish behavior. If we see the data for $L=36$ obtained at 5×10^4 MCS, the spin lengths are equal to $q \simeq 0.16$ and 0.47 at $T/J=0.30$ and 0.20, respectively, and q is considerably smaller than m_s in the low temperature phase. (Generally it is difficult to translate the Monte Carlo time into the real time because the Monte Carlo algorithm does not involve any real time scale. We expect, however, 5×10^4 MCS corresponds to a time scale much longer than the microscopic time scale associated with an elementary spin-flip process and gives a not so unreasonable estimation of the experimental time scale of NMR etc.) From experimental viewpoint, this observation suggests that NMR or Mösbauer spectroscopy might give a shorter spin length than the neutron scattering does in a dynamical sense. These results seem consistent with the experimental data for the series compounds VX_2 (X=Cl, B_r and I).[11-14] They also seem consistent with the experimental data for YFe MnO_4 where the neutron scattering data always indicate stronger ordering than the data of Mösbauer spectroscopy do.[15]

Of course, in comparing our results obtained in the present simulation with the experimental data for these substances, we must pay attention to several effects which has been discarded in the present idealized model, *e.g.*, the quantum effect,[29,30] three-dimensional effect and anisotropy. We believe, however, that our present observations for the AFT Heisenberg model give, at least partially, a possible interpretation of the puzzling features of the experimental data for triangular lattice Heisenberg antiferromagnets.[11-15]

Acknowledgements

The authors would like to thank Professor M. Suzuki, Professor H. Shiba, Professor K. Hirakawa, Professor T. Haseda, Professor M. Tanaka, Dr. K. Takeda, Dr. H. Kadowaki and Dr. K. Ebina for useful discussions. The numerical calculations have been performed with FACOM M190 of Laboratory of International Collaboration on Elementary Particle Physics at Tokyo University, ACOS 1000 of the Computer Center at Osaka University and FACOM M200 of Institute of Plasma Physics at Nagoya University. This study is supported in part by Grant-in-Aid from the Ministry of Education, Science and Culture.

Appendix

In this appendix, we derive the relation (3.2) on the basis of the vortex bound-unbound picture for the phase transition. In the low-temperature phase, all Z_2 vortices are tightly bounded forming vortex pairs. We express the

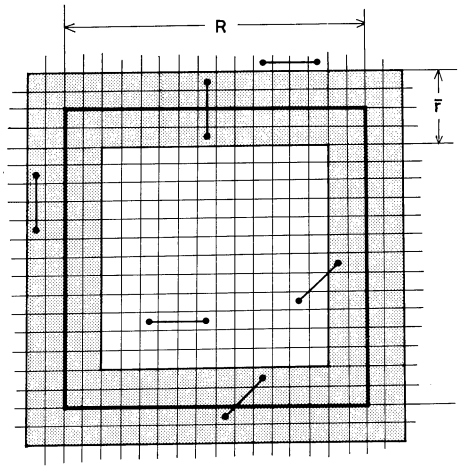

Fig. A1. An illustration of a closed contour with its perimeter R and the strip of width $\bar{r}$ along the contour. The system is assumed to be in the low-temperature phase ($T<T_c$), and all vortices form tightly bound vortex pairs with its separation $\bar{r}$.

separation of the members of a pair by $\bar{r}$ and consider a contour C with its perimeter $R\gg\bar{r}$. (See Fig. A1.) Recalling the conservation law of the vorticity, one can see that the vorticity for the contour C is equal to unity or minus unity depending on whether the number of elementary vortices contained in the contour is even or odd. Suppose a strip of width $\bar{r}$ along the contour which contains $N_R\propto R$, for the contour with square shape $N_R\simeq 4\bar{r}R$, plaquettes on the strip. We assume that, if the center of a vortex pair does not lie on this strip, the two vortices forming a pair is not cut by the contour. The vortex pairs outside the strip do not contribute to V_R and those inside the strip always give even number of elementary vortices, thus they actually do not contribute to V_R. Let us assume the probability that a unit plaquette on the strip has a vortex pair crossing the contour to be p. The probability that there are more than one vortex pair at a plaquette is small and we can neglect such probability. In the case we cannot neglect this probability, we redefine the p to be the probability of the event that there are odd number of vortex pairs crossing the contour at a unit plaquette. It should be noted that it is reasonable to assume $p<1/2$ in any case. Assuming that vortex pairs appear without correlation, we can evaluate the probability to have odd and even number of vortices in the contour to be

$$P_{\text{odd}}=\sum_{m=0} {}_{N_R}C_{2m+1}p^{2m+1}(1-p)^{N_R-2m-1},$$
$$P_{\text{even}}=\sum_{m=0} {}_{N_R}C_{2m}p^{2m}(1-p)^{N_R-2m}, \qquad (A\cdot 1)$$

so that

$$V_R=P_{\text{even}}-P_{\text{odd}}$$
$$=(1-2p)^{N_R}$$
$$=\exp\left[-\ln\frac{1}{1-2p}\cdot N_R\right]. \qquad (A\cdot 2)$$

Thus the perimeter law is derived.

In the high-temperature phase, a finite fraction of free vortices appear. First we consider the contribution of free vortices which is expected to give a dominant contribution to the decay of V_R. In this case, we have to count all vortices inside the contour in contrast to the case of $T<T_c$ where only margin plaquettes can cause odd number of vortices. Let p' be the appearance probability of free vortex at each unit plaquette. Assuming that free vortices appear without correlation, we get

$$V_R=\sum_{m=0} {}_{N_A}C_{2m}p'^{2m}(1-p')^{N_A-2m}$$
$$-\sum_{m=0} {}_{N_A}C_{2m+1}p'^{2m+1}(1-p')^{N_A-2m-1}, \qquad (A\cdot 3)$$

where $N_A\propto A$ is the total number of unit plaquettes in the contour. In this case, we obtain the area law as

$$V_R=(1-2p')^{N_A}=\exp\left[-\ln\frac{1}{1-2p'}N_A\right]. \qquad (A\cdot 4)$$

In the high-temperature phase, vortex pairs coexist with free vortices and cause an additional size dependence of V_R. But as far as the free vortex density is finite, the effect of vortex pairs is negligible in the limit $R\to\infty$.

References

1) G. Wannier: Phys. Rev. **79** (1950) 357 and **B7** (1973) 5017; R. M. F. Houtappel: Physica **16** (1950) 425; J. Stephenson: J. Math. Phys. **5** (1964) 1009.
2) S. Alexander and P. Pincus: J. Phys. **A13** (1980) 263.
3) M. Mekata: J. Phys. Soc. Jpn. **42** (1977) 76.
4) D. P. Landau: Phys. Rev. **B27** (1983) 5604.
5) H. Takayama, K. Matsumoto, H. Kawahara and K. Wada: J. Phys. Soc. Jpn. **52** (1983) 2888.
6) S. Fujiki, K. Shutoh, Y. Abe and S. Katsura: J. Phys. Soc. Jpn. **52** (1983) 1531; S. Fujiki, K.

Sthoch and S. Katsura: J. Phys. Soc. Jpn. **53** (1984) 1371.
7) J. Hosé, K. Kadanoff, S. Kirkpatrick and D. R. Nelson: Phys. Rev. **B16** (1977) 1217.
8) S. Miyashita and H. Shiba: J. Phys. Soc. Jpn. **53** (1984) 1145.
9) D. H. Lee, J. D. Joannopoulos, J. W. Negele and D. P. Landau: Phys. Rev. Lett. **52** (1984) 433.
10) H. Kawamura and S. Miyashita: J. Phys. Soc. Jpn. **53** (1984) 9.
11) K. Hirakawa, H. Kadowaki and K. Ubukoshi: J. Phys. Soc. Jpn. **52** (1983) 1814.
12) K. Hirakawa, H. Ikeda, H. Kadowaki and K. Ubukoshi: J. Phys. Soc. Jpn. **52** (1983) 2882.
13) I. Yamada, K. Ubukoshi and K. Hirakawa: J. Phys. Soc. Jpn. **53** (1984) 381.
14) K. Takeda, K. Ubukoshi, T. Haseda and K. Hirakawa: J. Phys. Soc. Jpn. **53** (1984) 1480.
15) M. Tanaka and K. Shiratori: private communication.
16) S. H. Shenker and J. Tobochnik: Phys. Rev. **B22** (1980) 4462.
17) G. Toulouse and M. Kléman: J. Phys. Lett. (France) **37** (1976) 149.
18) N. D. Mermin: Rev. Mod. Phys. **51** (1979) 591.
19) P. W. Anderson and G. Toulouse: Phys. Rev. Lett. **28** (1977) 508.
20) N. Rivier: Phil. Mag. **A40** (1979) 859.
21) K. G. Wilson: Phys. Rev. **D14** (1974) 2455; J. B. Kogut: Rev. Mod. Phys. **51** (1979) 659.
22) J. M. Kosterlitz and D. J. Thouless: J. Phys. **C6** (1973) 1181; J. M. Kosterlitz: J. Phys. **C7** (1974) 1046.
23) N. D. Mermin and H. Wagner: Phys. Rev. Lett. **17** (1966) 1133.
24) J. F. Fernández and T. S. J. Streit: Phys. Rev. **B25** (1982) 6910.
25) S. Miyashita, H. Nishimori, A. Kuroda and M. Suzuki: Prog. Theor. Phys. **60** (1978) 1669; S. Miyashita: Prog. Theor. Phys. **63** (1980) 797 and **65** (1981) 1595.
26) J. Tobochnik and G. V. Chester: Phys. Rev. **B20** (1979) 3761.
27) I. Morgenstern and K. Binder: Phys. Rev. Lett. **43** (1979) 1615, Phys. Rev. **B22** (1980) 288 and Z. Phys. **B39** (1980) 227.
28) D. Stauffer and K. Binder: Z. Phys. **B30** (1978) 313.
29) P. W. Anderson: Mater. Res. Bull. **8** (1973) 153; P. Fazekas and P. W. Anderson: Phil. Mag. **30** (1974) 423.
30) S. Miyashita: J. Phys. Soc. Jpn. **53** (1984) 44.